

SUPPORTING ONLINE MATERIAL (SOM)

Image Acquisition and Preprocessing:

High-resolution T1-weighted scans were acquired on Siemens 3T Allegra (TX) and Trio (CA) scanners using an MPRage sequence (Siemens). Functional run details: echo-planar imaging, gradient recalled echo; repetition time (TR) = 2000 ms; echo time (TE) = 40 ms; flip angle = 90°; 64 x 64 matrix, 26 4 mm axial slices, yielding functional 3.4 mm x 3.4 mm x 4.0 mm voxels.

Preprocessing of functional imaging data was performed using SPM2

(<http://www.fil.ion.ucl.ac.uk/spm/software/spm2>). Motion correction to the first functional scan was performed using a six-parameter rigid-body transformation (1). The average of the motion-corrected images was co-registered to each individual's structural MRI using a 12-parameter affine transformation. Slice timing artifact was corrected, after which images were spatially normalized to the MNI template (2) by applying a 12-parameter affine transformation, followed by a nonlinear warping using basis functions (3). Images were then smoothed with an 8 mm isotropic Gaussian kernel and highpass filtered in the temporal domain (filter width of 128s).

Statistical Analyses:

General linear model (GLM) analysis: Functional runs were divided into separate rounds that included all images preceding each round by 20 seconds and following each round by 30 seconds. Separate general linear models (4) were specified and estimated for each round of each subject. All visual stimuli and motor responses were entered as separate regressors that were constructed by convolving punctate events at the onset of each stimulus or motor response with the fixed hemodynamic response function implemented within SPM2.

The random-effects analyses depicted in figure 2B and Table 1 of SOM were performed as follows: Fixed-effects within trustee brains associated with the revelation of the investment were

used within a one-way analysis of variance. Specifically, contrast images generated from GLM analyses of 383 rounds were divided into 3 levels (benevolent, neutral, malevolent) of a single between-group factor (investor reciprocity), and comparisons between levels were performed. Rounds 1 and 2 were not included, as investor reciprocity cannot be calculated for initial rounds. Contrast 1 of SOM table 1 identifies four regions in which the activity of 10 or more voxels ($T(381)$, $p < .0001$, uncorrected) was greater in response to benevolent or malevolent reciprocity relative to neutral reciprocity. Contrasts of neutral reciprocity greater than benevolent or malevolent reciprocity did not identify any significant regions. Contrast 2 of SOM table 1 identifies the single region, head of caudate, in which activity in 10 or more voxels was greater ($T(247)$, $p < .001$, uncorrected) in response to benevolent reciprocity relative to malevolent reciprocity. Contrasts of malevolent reciprocity greater than benevolent reciprocity did not identify any significant regions.

The middle cingulate cortex (MCC) region identified in Figure 3A was identified with a one-sample t-test of fixed-effect contrasts for each round (submission of a subject's decision minus submission of partner's decision). The MCC activation (clustered around SPM coordinates: 0, 12, 40; $T = 16.03$) was the second most significantly activated region after visual cortex. The anterior cingulate cortex (ACC) region identified in Figure 3A was also determined by submitting fixed-effect contrasts for each round (revelation of partner's decision minus revelation of own decision) to a one-sample t-test. The ACC activation (clustered around SPM coordinates: 8, 40, -8; $T = 11.89$) was the third most significantly activated region after visual cortex and MCC.

Region of interest (ROI) analyses: ROI for all caudate analyses were performed on the 15 voxels most significantly activated in Contrast 2 of SOM Table 1. ROI analyses for ACC and MCC were performed on the 10 voxels most significantly activated in the GLM analyses described above. For each ROI, the preprocessed signal was averaged within the voxels of the ROI for each round. Second, the spatially averaged signal was linearly detrended within each round, and averages of multiple rounds were created by linearly interpolating and averaging signals time-locked to the

display of the investment to the trustee brain. The caudate activity illustrated in figure 2C is based on averages grouped by the level of reciprocity expressed at the investment ($\Delta I_j - \Delta R_{j-1}$; $t = 0$ sec). Caudate activity illustrated in figures 3 and 4 were grouped by the level trust (ΔR_j) expressed by the trustee at the subsequent repayment (repayment selection period begins at $t = 22$ sec). ACC and MCC activity illustrated in figure 3 was averaged across all rounds.

Correlograms: Correlograms were constructed by correlating signals (caudate, ACC, MCC) at different time shifts. Signals were averaged first and then correlated. For example, consider time shift = 0 for the blue traces of figure 3b. First, MCC signals and ACC signals was averaged separately for all rounds. Second, a correlation was made between 20 time-points (corresponding to -10 to +28 seconds relative to the submission of the investor's decision) of the ACC activity and the same 20 time-points of MCC activity. Correlations at 20 different time shifts are illustrated in each correlogram. In the case of the blue traces of figure 3, a positive time-shift corresponds to the shift forward in time of the MCC activity relative to the ACC activity. For example, a +4 sec time-shift corresponds to the correlation of average signal for -14 to +24 seconds (relative to submission of investor's decision) in the ACC with average signal for -10 to +28 seconds in the MCC.

SOM REFERENCES

1. K. J. Friston, S. Williams, R. Howard, R. S. J. Frackowiak, R. Turner, *Mag. Res. Med.* **35**, 346 (1996).
2. A. C. Evans et al. *Proc. IEEE-Nuclear Science Symposium and Medical Imaging Conference.* 1813 (1993)
3. J. Ashburner, K. J. Friston, *Hum. Brain Mapp.* **7**, 254 (1999).
4. K. J. Friston *et al.*, *Hum. Brain Mapp.* **2**, 189 (1995).
5. P. R. Montague *et al.*, *NeuroImage* **16**, 1159 (2002).

SOM FIGURE LEGENDS

SOM Figure 1. Diagram of hyperscanning during iterated trust game.

Within each pair, one subject was placed in a Siemens 3T Allegra scanner at Baylor College of Medicine (Houston, TX) and the other was placed in a Siemens 3T Trio scanner at Caltech (Pasadena, CA). Partner identity was kept strictly anonymous: subjects were given no information about their partner and did not meet or speak before, during, or after the task. Hyperscanning was performed with the use of NEMO 1.0 software (5). The freely available (open-source and platform-independent) software synchronizes: 1) scanning from multiple MRI locations; 2) presentation of stimuli to multiple subjects; and, 3) the acquisition of behavioral data from multiple subjects. The software can implement interactions among an arbitrary number of participants. The current release of NEMO implements the presentation of auditory (.wav), visual (.jpg, .avi), and gustatory stimuli, and the acquisition of mouse, keyboard, and MR compatible button-box responses. Synchronization is achieved through internet connections among multiple computers (server and client computers), and stimulation and acquisition can be achieved with timing precision of approximately +/-50 ms using broadband internet connections. Interested readers may contact nemo@hnl.bcm.tmc.edu and/or <http://www.hnl.bcm.tmc.edu/hyperScan.html> to obtain the current release of NEMO.

SOM Figure 2. Investment and repayment over course of trust game.

Mean and standard error of investment ratio (MU sent to trustee / 20) and repayment ratio (MU sent to investor / MU available to be sent) over the course of the trust game. Both investment and repayment ratios decreased as the end of the game approached, reflecting an unraveling of cooperation. Note in round 10, that investments did not earn a profit (green line indicates repayment ratio required to recoup investment).

SOM Figure 3. Behavioral summary of investor reciprocity subtypes.

Reciprocity events described in Figure 2A were segregated into additional categories reflecting the direction of change ($+\Delta I_r$, $-\Delta I_r$, $+\Delta R_{r-1}$, $-\Delta R_{r-1}$) that contributed to benevolent and malevolent reciprocity. Change in investment and repayment ratios are represented as vector angles within the following subcategories: for benevolent reciprocity: $+\Delta I_r, +\Delta R_{r-1}$; $+\Delta I_r, -\Delta R_{r-1}$; $-\Delta I_r, -\Delta R_{r-1}$; for malevolent reciprocity: $+\Delta I_r, +\Delta R_{r-1}$; $-\Delta I_r, +\Delta R_{r-1}$; $-\Delta I_r, -\Delta R_{r-1}$. Note that in each category, benevolent investor reciprocity results in an increase in subsequent repayment (indicated with the green arrows). Likewise, malevolent investor reciprocity results in a decrease in subsequent repayment (green arrows) for each category. This additional analysis indicates that the positive relationship between investor reciprocity and subsequent repayment ($r = .56$) is evident across reciprocity subtypes.

SOM Figure 4. Frequencies of benevolent, neutral and malevolent reciprocity within pairs.

Histograms reflect the number of benevolent, malevolent and neutral rounds evident within pairs. Pairs produced an average of 2.6 (SD=1.5) benevolent round, 2.8 (2.2) neutral rounds, and 2.6 (1.2) malevolent rounds.

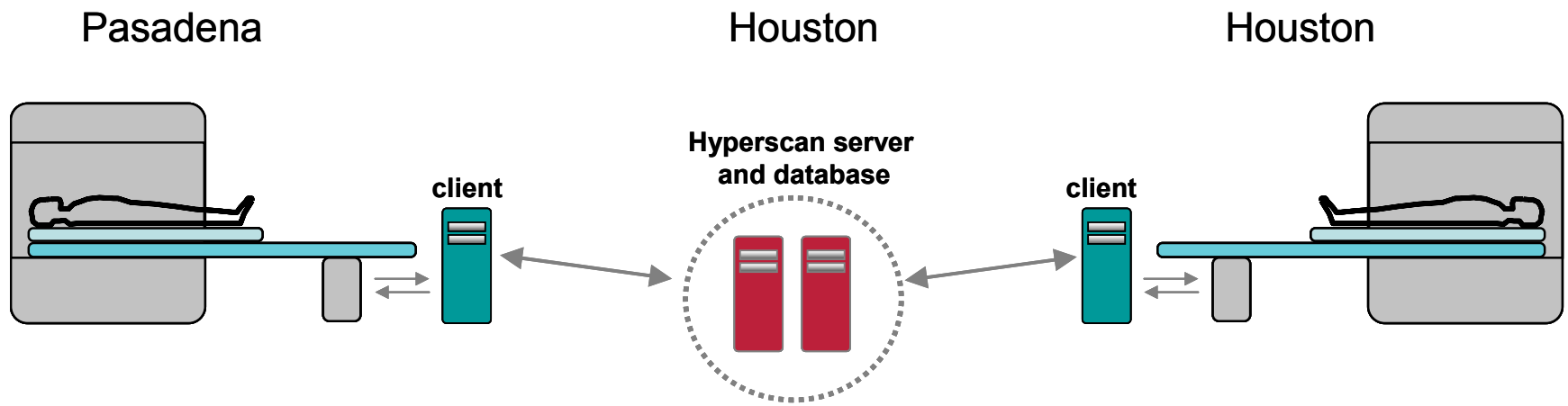
SOM Figure 5. Correlation of change in investment and change in next repayment. Two-tailed, nonparametric correlations (Spearman rho) of current change in investment (ΔI_j) and future change in repayment (ΔR_j) were computed for rounds 3 through 10 (corresponding to the rounds analyzed in the GLM for reciprocity). Of 384 investments, 173 did not differ from previous investments ($\Delta I = 0$) and were excluded from analysis. Consequently, rho degrees of freedom for each round ranged from 23 to 31. Significant relationships are indicated with * ($p < .05$) and ** ($p < .01$).

SOM Figure 6. Increase, not decreases, in repayment predict changes in next investment.

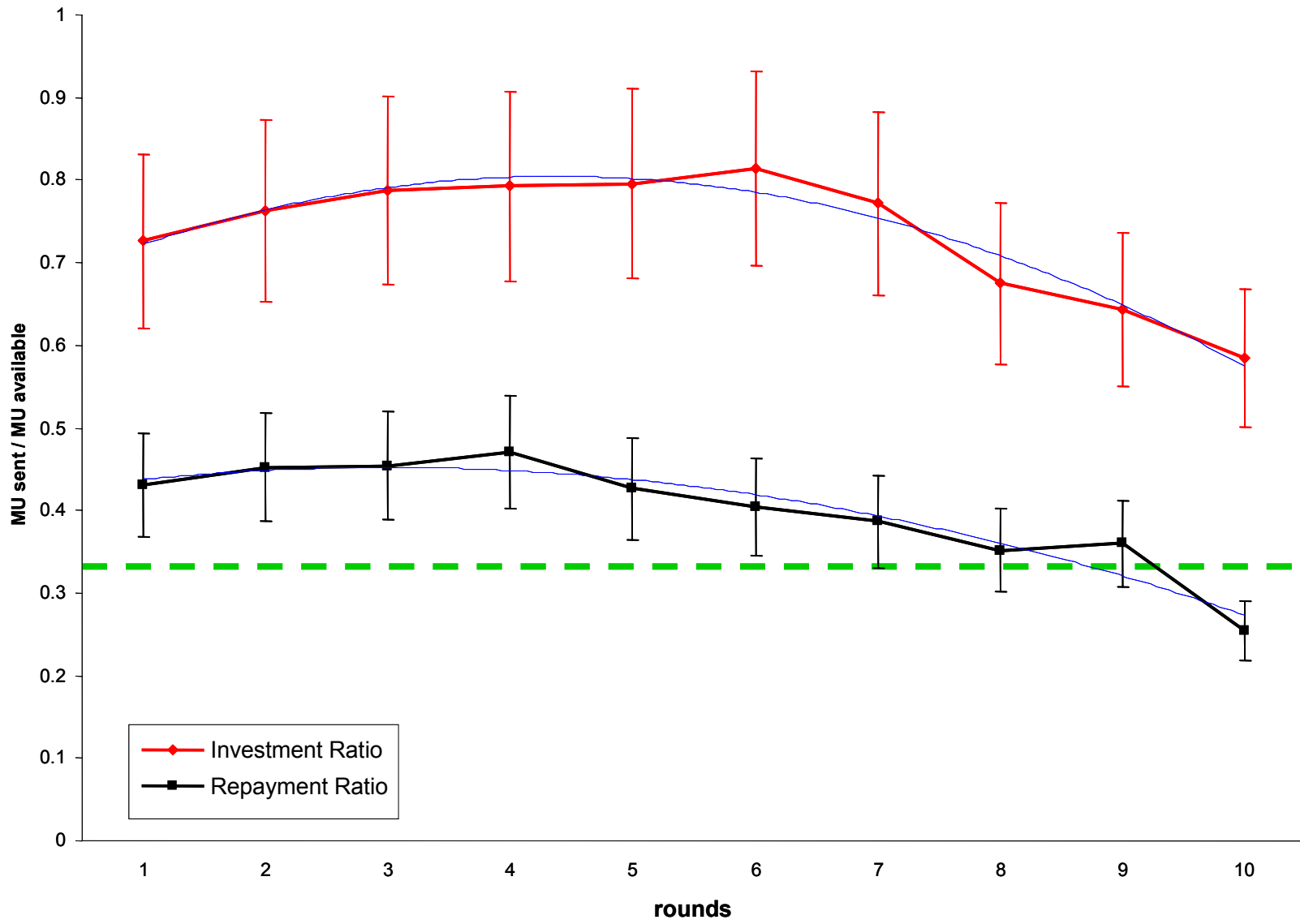
A. Scatterplot of increases in repayment and subsequent investment. Increases in repayment ($\Delta R_j > 5\%$) was moderately correlated ($r = .27$) with changes in next investment

(ΔI_{j+1}) . **B. Scatterplot of decreases in repayment and subsequent investment.** Decreases in repayment ($\Delta R_j < -5\%$) were uncorrelated ($r = .00$) with changes in next investment (ΔI_{j+1}).

SOM Figure 1

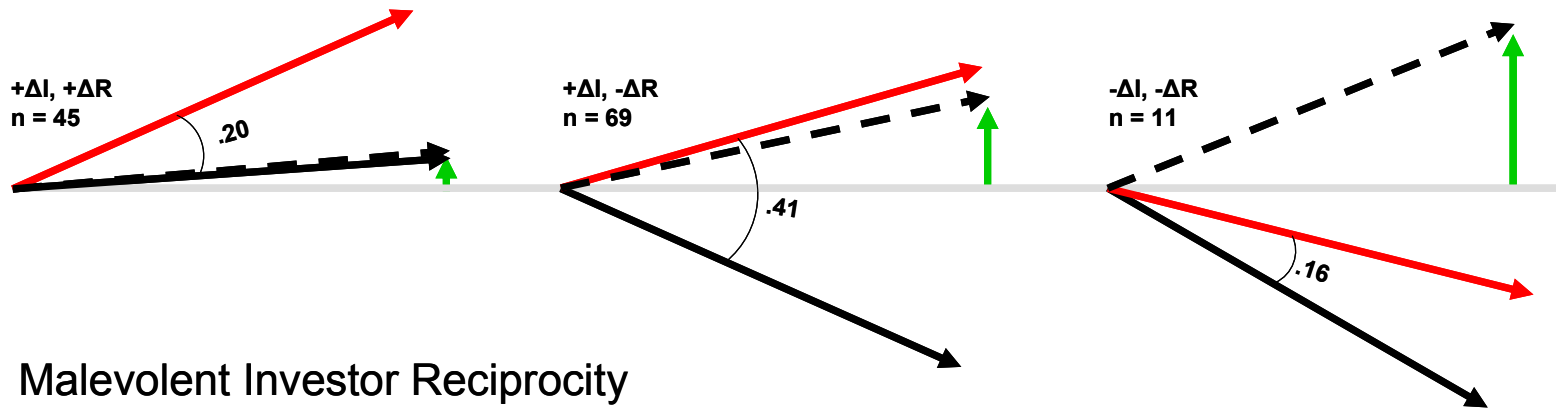


SOM Figure 2

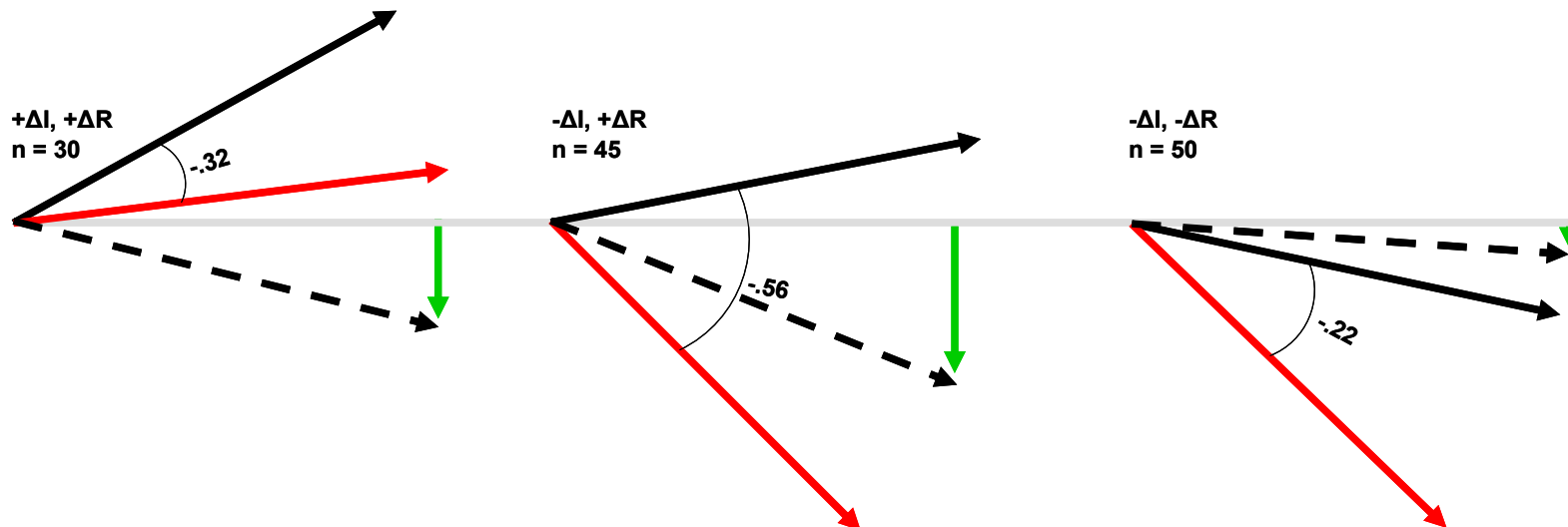


SOM Figure 3

Benevolent Investor Reciprocity



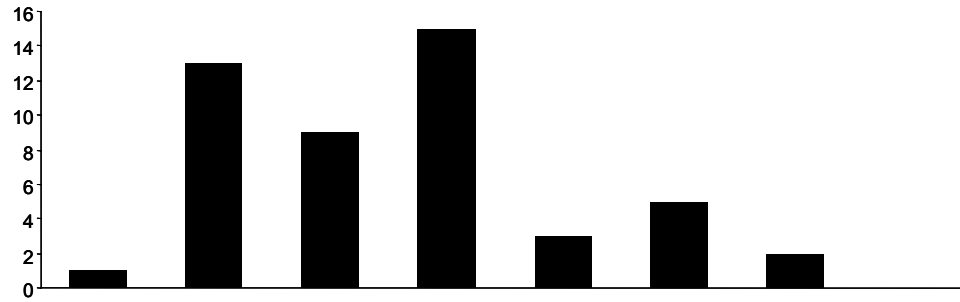
Malevolent Investor Reciprocity



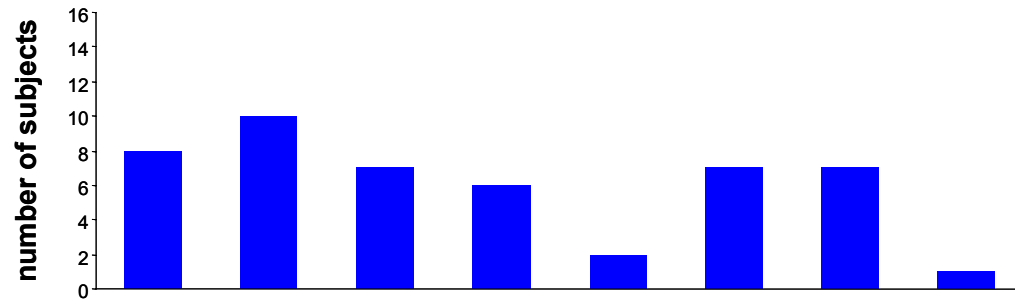
SOM Figure 4

Investor Reciprocity

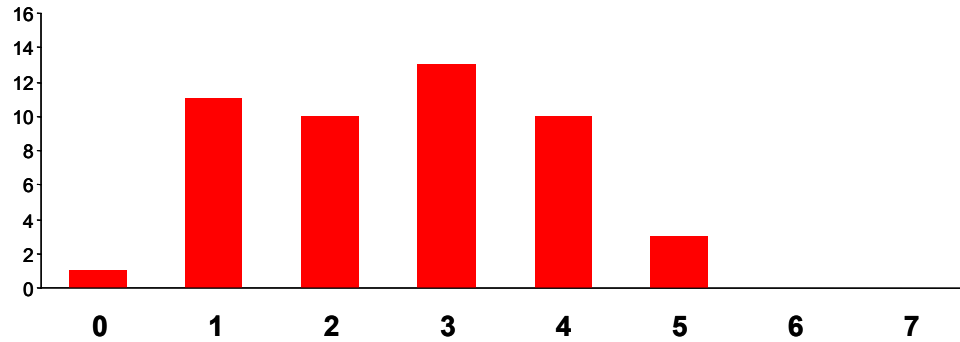
Benevolent
N = 125



Neutral
N = 134

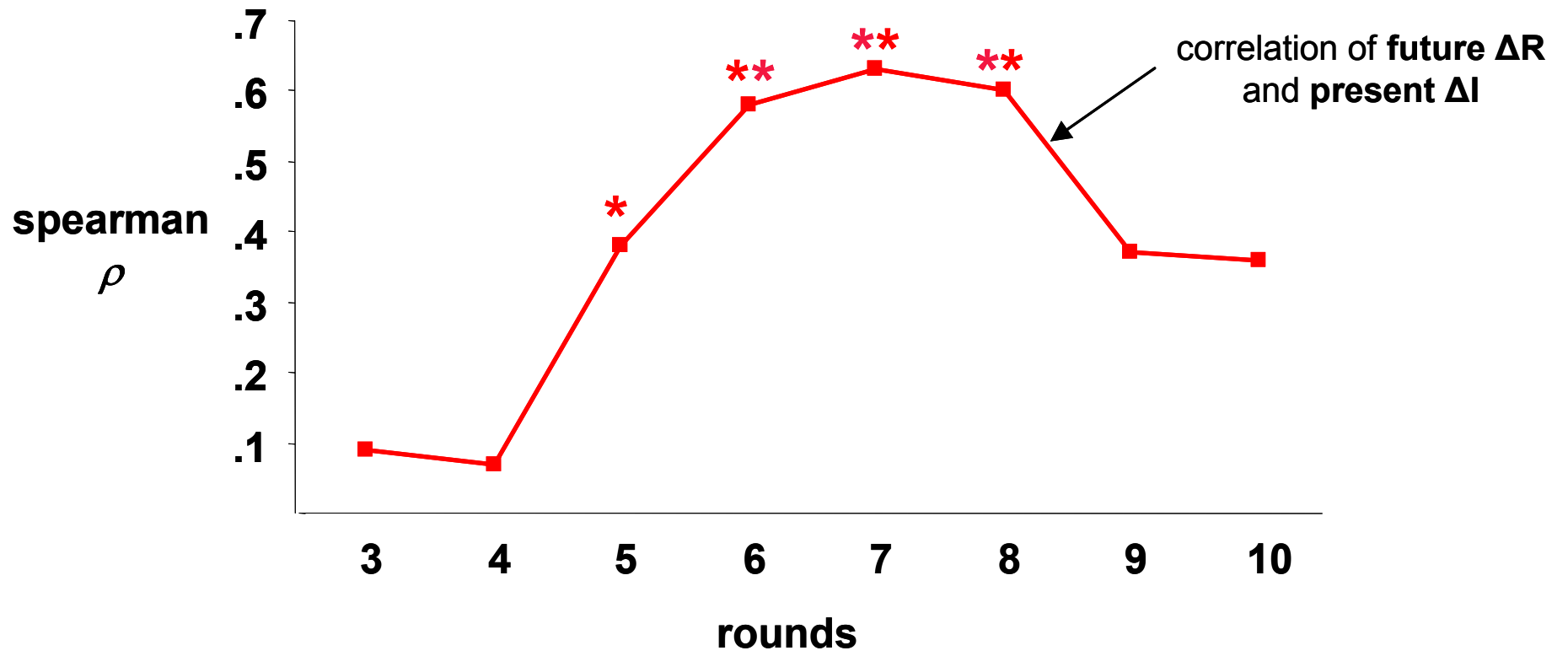


Malevolent
N = 125



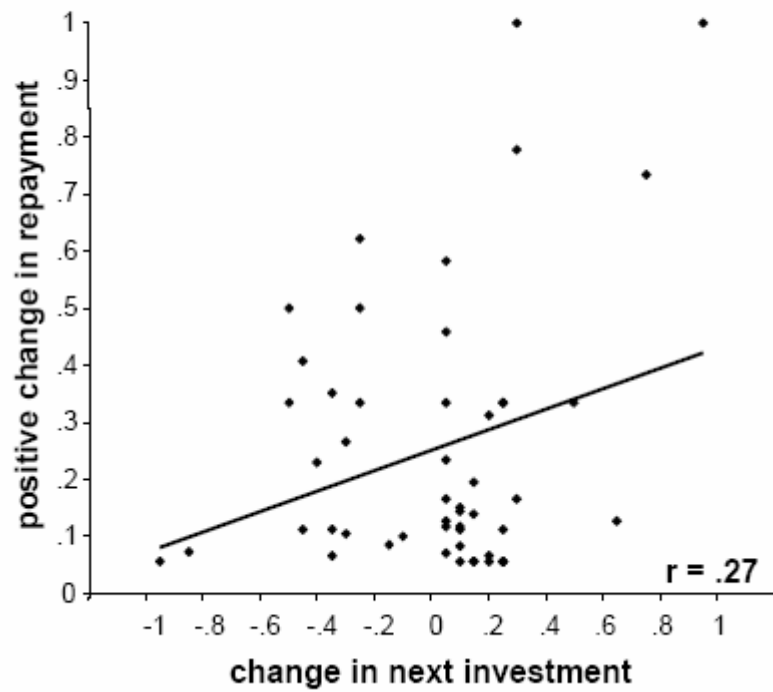
number of rounds

SOM Figure 5

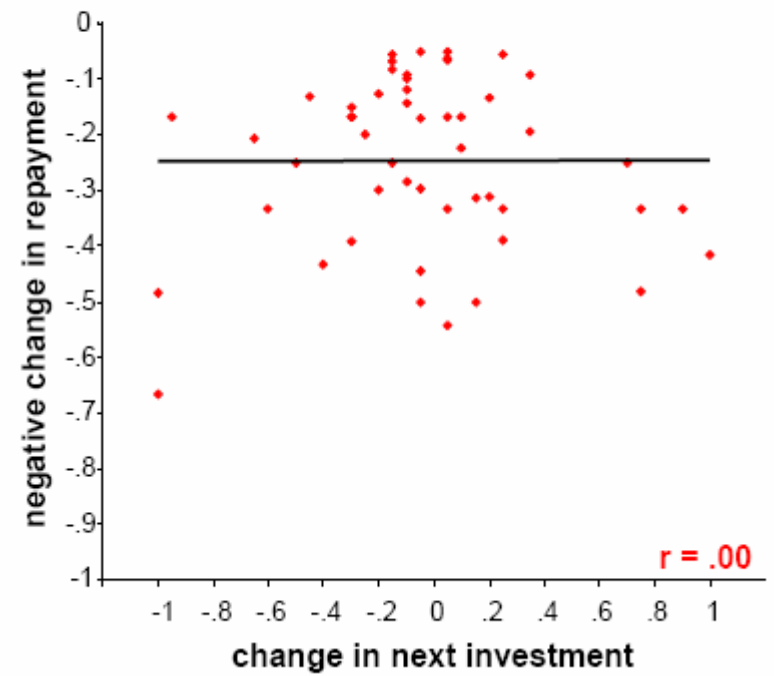


SOM Figure 6.

A



B



SOM TABLE LEGEND

SOM Table 1. Results of one-way analysis of variance for three levels of reciprocity.

Contrast images generated from GLM analyses of 383 rounds were divided into 3 levels (benevolent, neutral, malevolent) of a single between-group factor (investor reciprocity), and comparisons between levels were performed. Contrast 1 identifies four regions in which the activity of 10 or more ($T(381)$, $p < .0001$, uncorrected) was greater in response to benevolent or malevolent reciprocity relative to neutral reciprocity. Contrast 2 of SOM table 1 identifies the single region, head of caudate, in which activity in 10 or more voxels was greater ($T(247)$, $p < .001$, uncorrected) in response to benevolent reciprocity relative to malevolent reciprocity. The contrast of malevolent reciprocity greater than benevolent reciprocity did not identify any significant regions.

SOM Table 1.

SOM Table 1

Areas of trustee brain showing effect of investor reciprocity.

region of activation	laterality	x	y	z	T	Z
Contrast 1: benevolent or malevolent > neutral						
<i>subcortical</i>						
i/s colliculi	R	4	-28	-4	4.85	4.77
i/s colliculi	L	-8	-28	-8	5.00	4.92
thalamus	R	8	-4	0	5.64	5.52
thalamus	L	-8	0	0	5.80	5.68
<i>cortical</i>						
inferior frontal sulcus	R	-48	4	32	4.72	4.65
inferior frontal sulcus	L	48	8	28	4.54	4.47
superior frontal sulcus	R	-32	12	48	4.41	4.35
Contrast 2: benevolent > malevolent						
<i>subcortical</i>						
caudate	R	12	24	4	3.77	3.71
caudate	L	-8	20	4	3.25	3.22
<i>cortical</i>						
none	-	-	-	-	-	-

Levels of investor reciprocity consisted of 125 negative ($x < -.025$), 134 neutral ($-.025 \geq x \geq .05$), and 124 positive ($x > .05$) rounds.

Regions with 10 or greater significant voxels were identified using T-tests [Contrast 1 = T(381), $p < .0001$ (uncorrected); Contrast 2 = T(247), $p < .001$ (uncorrected)].